International Journal of Civil and Structural Engineering Research ISSN 2348-7607 (Online)
Vol. 3, Issue 2, pp: (174-184), Month: October 2015 - March 2016, Available at: www.researchpublish.com

Multiscale Stochastic Finite Element Modeling for Chloride Diffusion in Recycled Aggregate Concrete Using Digital Image Kernel

Samba Dia[1], Yu-Ching Wu[2]

[12]Structural Engineering Department, College of Civil Engineering, Tongji University, 200092, Shanghai, P.R. China

Abstract: **Increased deposition of construction waste in the environment and the continued depletion of the natural resources for construction raw material has led to the growing research on recycled aggregate concrete to find out and prove whether it can be as durable as natural aggregate concrete. Durability of this type of concrete is of great concern especially in harsh environments such as seawater environments, areas exposed to numerous freezing and thawing cycles and areas containing chemicals like Sulphates or Chlorides This paper presents a Multiscale Stochastic Finite Element Method that incorporates our newly developed digital image kernel for studying chloride diffusion in concrete and how it affects the durability of recycled aggregate concrete. The major focus of this study is to show the feasibility of our new digital image kernel, compare its development and application with other five selected kernels from literature and to highlight the advantages and disadvantages of this method.**

Keywords: **Recycled Aggregate Concrete, Multiscale Stochastic Finite Element Model, Karhunen-Loeve Theory, Chloride Diffusion, Digital Image Kernel.**

I. INTRODUCTION

The massive construction that has taken place around the world over the past years has led to generation of a great amount of construction waste, depletion of the natural earth for raw materials and a high cost of construction. Taking Taiwan as an example, it has been reported that they are struggling with a shortage of natural sand and gravel for concrete production. Fortunately, the use of Recycled Concrete Aggregate (RCA) presents a possible method to reduce the consumption of natural resources [1]. Recycled Aggregate Concrete (RAC) is not yet widely used because there still exists concern about its durability aspects. Chloride ions are one of the major factors that affect the durability of reinforced concrete. This is so because they have the ability to induce steel corrosion and concrete cover cracking [2]. Therefore, determining the chloride diffusivity of concrete is paramount however it is also quite difficult because it is influenced by many parameters such as the interfacial transition zone (ITZ) and the microstructure of the concrete (porosity and pore structure). These properties are present in RAC in a more complicated fashion and thus greatly influence the quality of RAC because they increase its susceptibility to diffusion of chloride ions [3].

Tam et al. [4] found that the microstructure of RAC was much more complicated than that of the conventional concrete because it possessed two ITZs, one is between the RCA and new mortar matrix, and the other is between the RCA and the old mortar attached (old ITZ). Additionally, Poon et al. [5] using a scanning electron microscope (SEM) revealed that the ITZ of RAC consisted mainly of loose and porous hydrates whereas the aggregate–cement matrix interfacial zone of conventional concrete consisted mainly of dense hydrates. Past researchers have proved that the absorption rates of recycled aggregate are higher compared to that of natural aggregate [6-7]. Kou et al [8] summarized that the chloride diffusion of RAC was 1.53 times more than that for NAC. This literature review, shows that chloride ion diffusion in RAC is greatly influenced by the uncertainty of its microstructure.

Additionally, the past two decades have proved the multiscale stochastic finite element method (MsSFEM) to be a very effective tool, because it takes into account material heterogeneity and material properties across different scales. From this we can obtain values that are near to the real situation as much as possible. Numerous research on MsSFEM has been carried out, of which only a few are employed in this paper including; homogenization theory [9,10], and multi-scale method [11-13] and stochastic analysis [14-16]. To use these multi-scale numerical model one of the relevant parts of stochastic processes is the Karhunen-Loeve (KL) expansion, which is a widely used method. The KL expansion can be broken down according to the following formula:

$$H(y,\varphi) = \mu(y) + \sum_{i=1}^{\infty} \sqrt{\lambda_i}\,\Psi_i(\varphi)\gamma_i(y) \quad (1)$$

Wherein, y, represents the micro-scale and φ is a random variable of the H arbitrary random function, μ is the average of the random function H, λ_i and γ_i are the eigenvalues and eigenvectors of the eigenvalue problem as shown below.

$$\int_Y C(y,y')\gamma_i(y')dy' = \lambda_i\gamma_i(y) \quad (2)$$

The kernel $C(y,y')$ is the covariance function of $H(x,\varphi)$ defined by,

$$C(y,y') = E[(H(y,\varphi)-\mu(y))(H(y',\varphi)-\mu(y'))] = \sum_{i=1}^{\infty}\lambda_i\gamma_i(y)\gamma_i(y') \quad (3)$$

In addition, Ψ_i represents the standard definite polynomial variables.

In most of the literature, there are two major ways to start solving the Karhunen-Loeve expansion which are the mathematical method and the numerical method.

In the mathematical method, a standard kernel is selected then according to the autoregression eigenanalysis of a random value projected onto the covariance we use mathematical expressions to obtain eigenvalues and eigenvectors. This method is very taxing for many non-mathematical staff in the engineering field. The Markov kernel is set here as an example, then mathematical methods are used for solving integral equation eigenvalue problem. The Markov kernel can be written as

$$C(x,x') = e^{-|x-x'|/b} \quad (4)$$

Suppose the random process is defined in one dimension domain, from -a to a, the differential equations can be written as

$$\int_{-a}^{a} e^{-c|x-x'|} f(x')dx' = \lambda f(x) \quad (5)$$

Where c = 1 / b, decomposing the formula into two parts, -a to x and x to a. With the conduction of two simultaneous derivations of x, we obtain the following formula

$$f''(x) + \omega^2 f(x) = 0 \quad -a \le x \le a \quad (6)$$

Where

$$\omega^2 = \frac{2c - c^2\lambda}{\lambda}$$

Boundary condition is

$$cf(a) + f'(a) = 0$$

$$cf(-a) - f'(-a) = 0$$

Solve the equation can we get two roots ω and ω *, the characteristic equation for the even I and odd i is

$$f_i(x) = \frac{\cos(\omega_i x)}{\sqrt{a + \dfrac{\sin(2\omega_i a)}{2\omega_i}}}$$

$$f_i^*(x) = \frac{\sin(\omega_i^* x)}{\sqrt{a - \frac{\sin(2\omega_i^* a)}{2\omega_i^*}}}$$

Corresponding eigenvalues is

$$\lambda_i = \frac{2c}{\omega_i^2 + c^2}$$

$$\lambda_i^* = \frac{2c}{\omega_i^{*2} + c^2}$$

In the numerical method, the eigenvalue problem, through certain basis functions, is converted to a matrix equation in order to solve the eigenvectors and eigenvalues of the covariance function. We use a basis function $h_i(x)$ and make it a complete series of equations Hilbert space. The characteristic equation can be approximated to

$$f_k(x) = \sum_{i=1}^{N} d_i^k h_i(x) \quad (7)$$

Substituting to the original integral equation Eq. (5), the error ε_N can be written as

$$\varepsilon_N = \sum_{i=1}^{N} d_i^k \left[\int C(x,x') h_i(x') dx' - \lambda\, h_i(x) \right] \quad (8)$$

This error must be orthogonal with this approximation space, which can be written as

$$\left(\varepsilon_N, h_j(x)\right) = 0, \quad j = 1, \ldots, N \quad (9)$$

We express it in the form of a matrix

$$\mathbf{CD} = \mathbf{\Lambda BD} \quad (10)$$

In which

$$\mathbf{C}_{ij} = \int\int C(x,x') h_i(x) h_j(x') dx dx'$$

$$\mathbf{B}_{ij} = \int h_i(x) h_j(x) dx$$

$$\mathbf{D}_{ij} = d_i^j$$

$$\mathbf{\Lambda}_{ij} = \lambda \delta_{ij}$$

Solving the eigenvalue problem Eq. (10) and we obtain eigenvalues λ and eigenvectors d_i^j, this eigenvectors cannot be used directly; it must be substituted back to Eq. (7) which finally leads to the mathematical expression of eigenvectors.

In this paper we focus on the use of digital image processing (DIP) techniques to develop a new digital image kernel (DIK). We do this by using pixels of the microscopic image of our RAC and inserting them into our kernel equation. This method skips the complex processes experienced in the previously described methods. Our new method is quite simple and therefore convenient for non-engineering staff because i we use the pixels of the image directly onto the kernel to obtain useful results.

The main objective of this paper is to explore the MsSFEM combined with this digital image kernel, the feasibility in the application of the DIK and the advantages and disadvantages of the development and implementation of digital image kernel in MsSFEM for the study of chloride diffusion in RAC.

II. METHODOLOGY

A. Eigenanalysis of AR (1) process:

Signal models including autoregressive (AR), moving average (MA), and autoregressive moving average (ARMA) types are often used to mathematically describe random processes and information sources. In particular, the first-order AR model, AR (1), which is a first approximation to many natural signals, is used here. It has been successfully employed in the modeling of digital images which is why we chose to use it here. Generation of the AR (1) signal is begins with the first-order regression formula written as

$$\xi(n) = \xi_0(n) + \rho\xi(n-1) \quad (11)$$

Wherein, $\xi_0(n)$ is a random series possessing zero-mean standard deviation, with real numbers ranging from -1 <ρ <1. The variance of $\xi(n)$ is given as follows

$$\sigma_\xi^2 = \frac{1}{1-\rho^2} \quad (12)$$

Covariance series of $\xi(n)$ is

$$R_{\xi\xi}(k) = E[\xi(n)\xi(n+k)] = \sigma_\xi^2 \rho^{|k|} \quad (13)$$

The size of the covariance matrix R_ξ is N × N, which must satisfy Eigenequation

$$R_\xi = \sigma_\xi^2 \begin{bmatrix} 1 & \rho & \rho^2 & \cdots & \rho^{N-1} \\ \rho & 1 & \rho & \cdots & \rho^{N-2} \\ \rho^2 & \rho & 1 & \cdots & \rho^{N-3} \\ \vdots & \vdots & \vdots & \ddots & \vdots \\ \rho^{N-1} & \rho^{N-2} & \rho^{N-3} & \cdots & 1 \end{bmatrix} \quad (14)$$

The steps involved in this paper to solve the intergral equation of the eigenvalur problem are based on [17] by Torun and Akansu. Their method followed three basic steps which we implemented in our study. Firstly, the statistical measurement of the random vector process was first carried out using MATLAB software in order to obtain the covariance matrix. Then, the eigenvectors and eigenvalues for the given covariance matrix are calculated. Finally, incoming random signal vector is mapped to the eigenspace (subspace) by using the pre-calculated eigenmatrix for the given covariance matrix. Details of this are explained further below:

A microscope linked to a Nikon Coolpix 990 digital camera is used to obtain high quality images. Many photos of the RAC sample were taken to obtain statistical sample data. We then employed the MATLAB software for image reading and to convert it to a gray scale image of which figure 1 is an example. From here, we are able to extract the pixel gray matrix which involves the information used in the digital image Covariance Kernel.

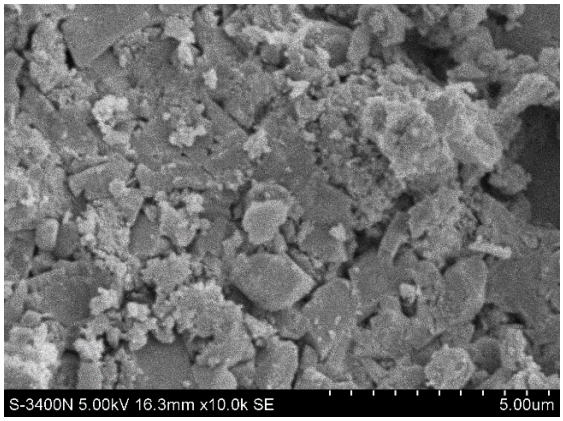

Fig. 1 One of the digital images of the RAC sample

B. Covariance matrix calculation:

The grayscale image pixel matrix of the RAC sample is extracted from the picture using MATLAB software. An appropriate matrix size 800 × 800 was chosen and according to the following theory, we formulate covariance calculations:

A set of linearly independent orthogonal discrete random series Θ numbered n , in the interval $1 \le i, j, k \le N$ satisfies the orthogonality of discrete Fourier transform and likewise by forward-change operation we map the orthogonality of the matrix to the Orthogonal Space. Covariance matrix and variance array are defined as follows:

$$\mathbf{C}_{ij} = E[(\Theta_i - \mu_i)(\Theta_j - \mu_j)^T] \quad (15)$$

$$\sigma_i^2 = \frac{1}{N}\sum_{k=1}^{N}\sigma_{ik}^2 \quad (16)$$

From the covariance matrix above, the eigenvalue equation can be written as

$$\mathbf{C\Phi} = \lambda\mathbf{\Phi} \quad (17)$$

Thus we can directly obtain the eigenvalues and eigenvectors.

Since the size of eigenvalues and eigenvectors is taken from the number of pixels we do not know the mathematical expression of eigenvectors, but the interval between pixels is very small, and the result is almost continuous. If one needs to calculate values between pixels, the interpolation can be used, even without interpolation and instead using approximate solutions directly on either side, the error will be very small, which is within the allowable range. This shows that this method step is very simple and straightforward. The value of approximation error in Monte-Carlo expansion is as follows

$$\varepsilon = C(x,x') - \sum_{i=1}^{num}\lambda_i f_i(x) f_i(x') \quad (18)$$

Where num is the number of selected Carlo expansion series.

C. Multiscale finite element analysis of chloride ion diffusion in RAC:

In this study, the aggregates were generally considered to be impermeable, the mortar heterogeneous and the fine aggregates, voids, and cracks were assumed to be mixed up with the cement paste establishing the matrix phase. Microscopic uncertainties of both the old and new ITZ were accounted for thus; the homogenized diffusion coefficient of ITZ had to be computed through stochastic process while the diffusivity of the mortar matrix was attained by homogenization. Based on Zheng and Zhou's [18] investigation, the expression of the chloride diffusion coefficient *D* takes the form as

$$D = \frac{2V_p^{2.75}D_p}{V_p^{2.75}\left(3 - V_p\right) + n\left(1 - V_p\right)^{2.75}} \quad (19)$$

Where V_p is the overall porosity, D_p is the is the effective diffusivity and n is the porosity of the concrete.

The chloride diffusion coefficient tensor can be defined as

$$D^{\beta}(x) = D(y) \quad (20)$$

Wherein, x is coarse scale coordinates, y coordinates for the thin gauge, the relationship is $x = y / \beta$.

Chloride diffusion equation can be written as

$$\nabla \cdot \left(D^{\beta}\nabla\zeta\right) + Q = 0, \qquad x \in \Omega \quad (21)$$

The boundary condition is given as

$$\zeta^{\beta} = 0, \qquad x \in \partial\Omega$$

D. Variational Formulation for Multiscale methods:

$$\alpha^{\beta}(\zeta, \eta)$$

A bilinear form of $\alpha^{\beta}(\zeta, \eta)$ is considered to be defined as follows

$$\alpha^{\beta}(\zeta^{\beta}, \eta) = \int_{\Omega} \nabla \eta D^{\beta} \nabla \zeta dx \quad (22)$$

And a following linear form

$$L(\eta) = \int_{\Omega} \eta Q dx + \int_{\partial\Omega} \eta q dx \quad (23)$$

The variational statement equivalent to the chloride diffusion problem is obtained by finding ζ^{β} which fulfills the following equation:

$$\alpha^{\beta}(\zeta^{\beta}, \eta) = L(\eta) \quad (24)$$

The above formula can be decomposed into

$$\int_{\Omega}\int_{Y} (\nabla\zeta + \nabla_y\zeta) D^{\beta} (\nabla\eta + \nabla_y\eta) dy dx = \int_{\Omega} \eta Q dx + \int_{\partial\Omega} \eta q dx \quad (25)$$

Which leads to the following expressions

$$\int_{\Omega}\int_{Y} (\nabla\zeta + \nabla_y\zeta) D^{\beta} \nabla_y \eta dy dx = 0 \quad (26)$$

$$\int_{\Omega}\int_{Y} (\nabla\zeta + \nabla_y\zeta) D^{\beta} \nabla \eta dy dx = \int_{\Omega} \eta Q dx + \int_{\partial\Omega} \eta q dx \quad (27)$$

Formula (34) can therefore be expressed as

$$\int_{Y} \nabla_y \zeta D^{\beta} \nabla_y \eta dy = -\int_{Y} \nabla \zeta D^{\beta} \nabla_y \eta dy \quad (28)$$

This equation itself is the weak form of random variational problems which can be solved by spectral stochastic finite element method proposed in the next unit, with a solution of corresponding chloride concentration values ζ. Substituting to formula (35) we can obtain the available chlorine ion diffusion coefficient

$$D^{(\mathbf{eff})} = \frac{1}{|Y|} \int_{Y} \big(D(y) + D(y)\nabla\Phi(y)\big) dy \quad (29)$$

E. Spectral Stochastic Finite Element Method:

In order to solve the formula (28), we require the spectral stochastic finite element method, therefore, a brief introduction to it is given below. Here, the chloride ion diffusion coefficient is defined as a random parameter, which can be written as

$$\hat{D}(y, \varphi) = H(y, \varphi)\hat{D}_0 \quad (30)$$

Where H (y, φ) is defined in (1), and by implementing formula (30) into equation (27) can we obtain

Using the theory that error is orthogonal to the approximate space, then

$$\sum_{i=0}^{P-1} \hat{D}_{ik} \Phi_i = Q_k \qquad k = 0, \cdots, P-1 \quad (31)$$

Wherein

$$\hat{D}_{jk} = \sum_{i=0}^{M} d_{ijk} \hat{D}_i \quad (44)$$

$$Q_k = \sum_{i=0}^{M} c_{ik} Q_i \quad (45)$$

Here

$$d_{ijk} = E[\Psi_i \Psi_j \Psi_k]$$

$$c_{ik} = E[\Psi_i \Psi_k] \quad (46)$$

Whereby M is the order of homogeneous chaos expansions while P is the number of polynomial chaos expansions.

F. numerical experiments:

In this section, we employed 5 five general kernel from literature to make comparison with our new kernel. Table 1 is a summary of all the kernels used.

Table 1 Equations Formulation for different Kernels

b	Kernel Name	Equations Formulation
1	Exponential Covariance Kernel	$e^{-a\|x-x'\|}$
2	Triangular Covariance Kernel	$1-a\|x-x'\|$
3	Modified Exponential Covariance Kernel	$e^{-a\|x-x'\|}(1-a\|x-x'\|)$
4	Nataf Uniform Covariance Kernel	$2\sin(\pi/6\times e^{-a\|x-x'\|})$
5	Nataf Step Covariance Kernel	$2\sin(\pi/2\times e^{-a\|x-x'\|})$
6	Digital Image Covariance Kernel	NA

Feasibility Analysis :

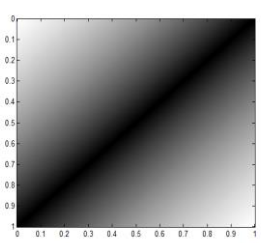

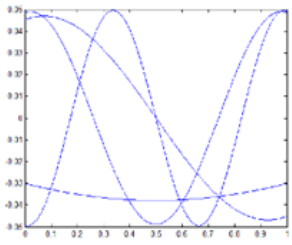

Fig. 2 The binary image of the Exponential Covariance Kernel **(a)**

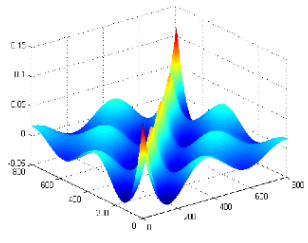

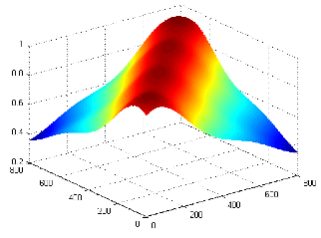

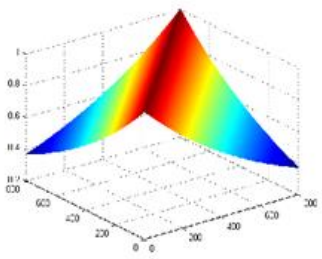

(b) **(c)** **(d)**

Fig. 3 The 4-term approximation for the Exponential Covariance Kernel: (a) Eigenfunctions; (b) Relative error surface; (c) Covariance surface; (d) Exact covariance surface.

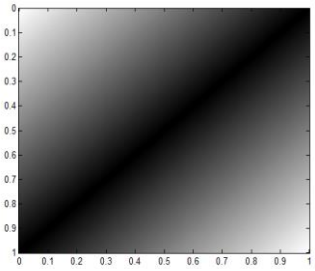

Fig. 4 The binary image of the triangular covariance kernel

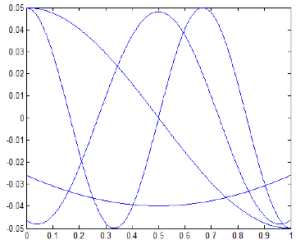

(a)

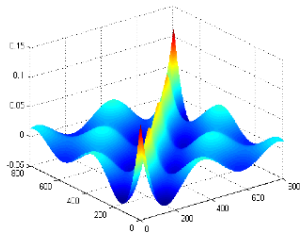

(b)

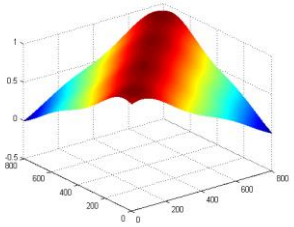

(c)

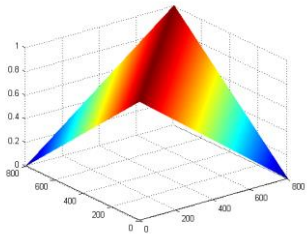

(d)

Fig. 5 The 4-term approximation for the triangular covariance kernel:
(a) Eigenfunctions; (b) Relative error surface; (c) Covariance surface; (d) Exact covariance surface

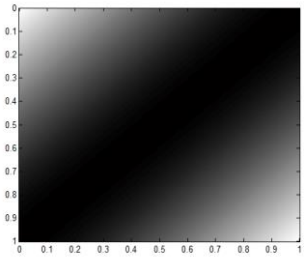

Fig 6 The binary image of the Modified Exponential Covariance Kernel

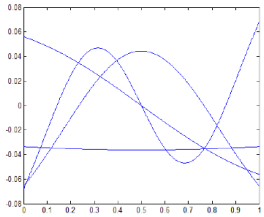

(a)

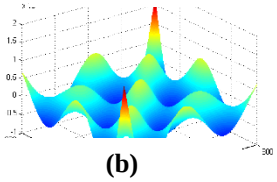

(b)

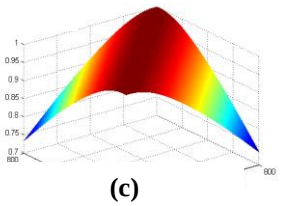

(c)

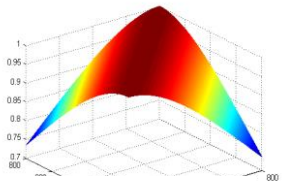

(d)

Fig. 7 The 4-term approximation for the Modified Exponential Covariance Kernel:

(a) Eigenfunctions; (b) Relative error surface; (c) Covariance surface; (d) Exact covariance surface

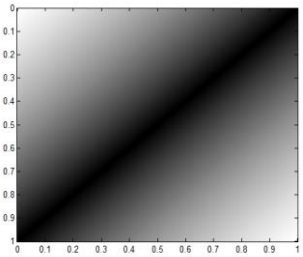

Fig 8 The binary image of the Nataf Uniform Covariance Kernel

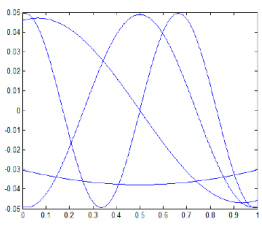

(a)

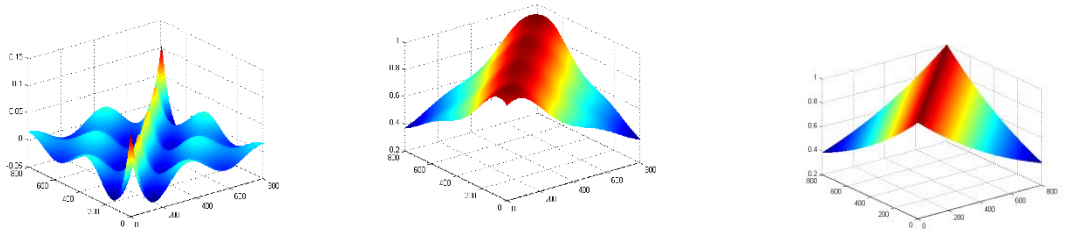

(b) (c) (d)

Figure 9 The 4-term approximation for the Nataf Uniform Covariance Kernel:
(a) Eigenfunctions; (b) Relative error surface; (c) Covariance surface; (d) Exact covariance surface

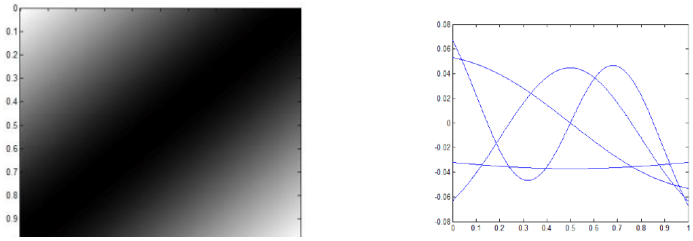

Fig. 10 The binary image of the Nataf Step Covariance Kernel

(a)

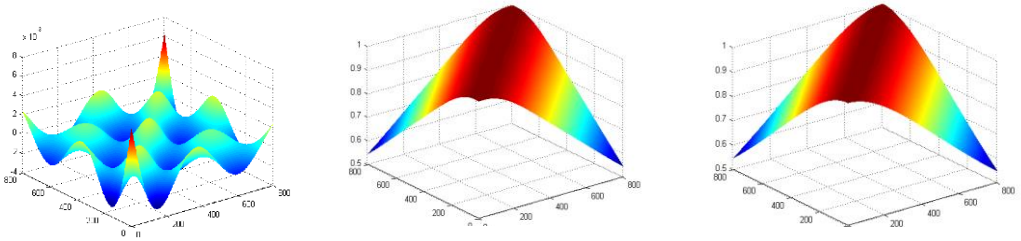

(b) (c) (d)

Fig. 11 The 4-term approximation for the Nataf Step Covariance Kernel:
(a) Eigenfunctions; (b) Relative error surface; (c) Covariance surface; (d) Exact covariance surface

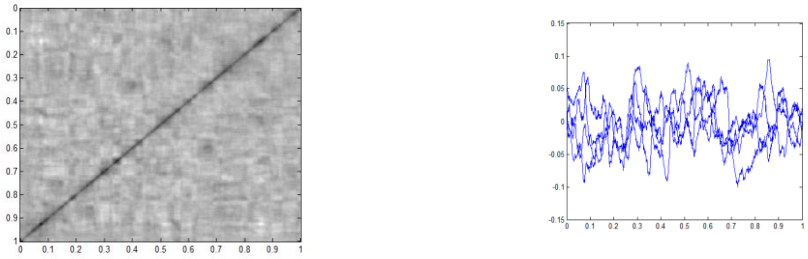

Fig. 12 The binary image of the Digital Image Covariance Kernel

(a)

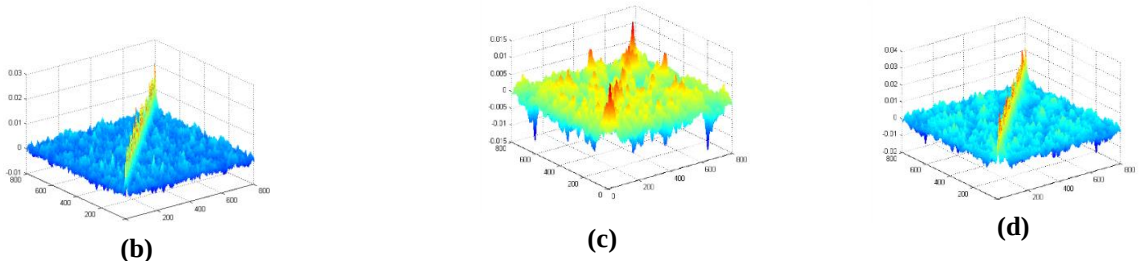

(b) (c) (d)

Fig.13 The 4-term approximation for the Digital Image Covariance Kernel:
(a) Eigenfunctions; (b) Relative error surface; (c) Covariance surface; (d) Exact covariance surface

Accuracy analysis:

In this section, we will compare the maximum error, the average error, computational time and memory of each kernel.

Table 2. Comparison of the maximum error

	Kernel Name	4th term Approximation
1	Exponential covariance kernel	0.1117
2	Triangular covariance kernel	0.1110
3	Modified exponential covariance kernel	0.0017
4	Nataf uniform covariance kernel	0.1021
5	Nataf step covariance kernel	0.0060
6	Digital image covariance kernel	0.000005

Table 3. Comparison of average error

	Kernel Name	4th term Approximation
1	Exponential covariance kernel	0.0129
2	Triangular covariance kernel	0.0130
3	Modified exponential covariance kernel	0.0002
4	Nataf uniform covariance kernel	0.0118
5	Nataf step covariance kernel	0.0008
6	Digital image covariance kernel	0.0000004

Table 4. Comparison of computer run time (unit: seconds)

	Kernel Name	6th term Approximation
1	Exponential covariance kernel	1.3166
2	Triangular covariance kernel	1.0228
3	Modified exponential covariance kernel	1.0460
4	Nataf uniform covariance kernel	1.0391
5	Nataf step covariance kernel	1.0370
6	Digital image covariance kernel	0.9806

Table 5. Comparison of computational memory (Unit: MB)

	Kernel Name	6th term Approximation
1	Exponential covariance kernel	2610
2	Triangular covariance kernel	2444
3	Modified exponential covariance kernel	2447
4	Nataf uniform covariance kernel	2452
5	Nataf step covariance kernel	2466
6	Digital image covariance kernel	2461

Table 2-5 shows that digital image kernel is much better than the other kernels in in accuracy and efficiency.

III. CONCLUSION

Recycled Aggregate concrete has shown to have a very varied microstructure which is why we employ both digital image processing techniques and the Multiscale Stochastic Finite Element Method. In this paper, digital image kernel method has been successfully applied to the multiscale stochastic finite element analysis of chloride diffusion in recycled aggregate concrete. In both its derivation and application, digital image kernel has shown very attractive properties. From the results we can summarize that, the proposed DIK has proven to be feasible, likewise, the digital image kernel has shown numerous advantageous properties over other selected kernels that were used for this paper including: much

simpler to derive, more accurate, more pervasive, requires shorter machine running time and less computer memory. The method is also very straight forward because it does not require complex formulations as used by other kernels. The advantages of the proposed kernel prove it to be a more than suitable kernel for the accurate analysis of chloride diffusion in concrete structures.

REFERENCES

[1] Ashraf M. Wagih, Hossam Z. El-Karmoty, Magda Ebid, Samir H. Okba "Recycled construction and demolition concrete waste as aggregate for structural concrete." HBRC Journal 9(2013), 193–200

[2] G. F. Kheder, S. A. Al-Windawi, "Variation in mechanical properties of natural and recycled aggregate concrete as related to the strength of their binding mortar" Materials and Structures 38(2005), 701-709.

[3] Yeong-Nain Sheen, Her-Yung Wang, Yi-Ping Juang, Duc-Hien Le, "Assessment on the engineering properties of ready-mixed concrete using recycled aggregates", Construction and Building Materials, 45(2013), 298–305.

[4] S R Yadav , S R Pathak "Use of recycled concrete aggregate in making concrete- an overview" 34th Conference on OUR WORLD IN CONCRETE & STRUCTURES, Singapore: (2009)16 – 18

[5] Xianming Shia, Ning Xiec, Keith Fortunea, Jing Gongd "Durability of steel reinforced concrete in chloride environments: An overview" Construction and Building Materials 30(2012), 125–138

[6] Ö. Çakır "Experimental analysis of properties of recycled coarse aggregate (RCA)concrete with mineral additives" Construction and Building Materials 68(2014), 17–25

[7] *Recycling of Demolished Concrete and Masonry*; Hansen, T.C., Ed.; Taylor and Francis: Oxfordshire, UK, 1992; p. 316.

[8] Vivian W.Y. Tam , X.F. Gaob, C.M. Tam "Microstructural analysis of recycled aggregate concrete produced from two-stage mixing approach" Cement and Concrete Research, 35(2005),1195–1203

[9] C.S. Poon, S.C. Kou, and L. Lam, "Use of recycled aggregate in moulded concrete bricks and blocks", *Construction and Building Materials*, 16(2002), 281–289.

[10] Peng C.L., D.E. Scorpio, and C.J. Kibert, "*Strategies for successful construction and demolition waste recycling operations."* Journal of Construction Management and Economics 15(1997), 49-58.

[11] Kou, S.C, Poon C.S, Chan D "Influence of fly ash as cement replacement on the properties of recycled aggregate concrete Journal of Materials in Civil Engineering", ASCE 19(2007), 709-717.

[12] Shayan, A., and Xu, A. (2003 Performance and properties of structural concrete made with recycled concrete aggregate ACI Mater. J., 100(5), 371 380, American Concrete Institute, Farmington Hills , USA.

[13] Kong, D.; Lei, T.; Zheng, J.; Ma, C.; Jiang, J.; Jiang, J. "Effect and mechanism of surface-coating pozzalanics materials around aggregate on properties and ITZ microstructure of recycled aggregate concrete" Construction and Building. Materials. 24 (2010), 701–708.

[14] George Stefanou "The stochastic finite element method: Past, present and future" Comput. Methods Appl. Mech. Engrg. 198(2009), 1031–1051

[15] R.E. Caflisch "Monte Carlo and quasi-Monte Carlo methods" Acta Numer 7(1998), 1–49.

[16] G.I. Schueller "A state-of-the-art report on computational stochastic mechanics" Probab. Engrg. Mech., 12 (4) (1997), 197–321

[17] Torun, M. U., and Akansu, A. N. "An Efficient Method to Derive Explicit KLT Kernel for First-Order Autoregressive Discrete Process" IEEE Transactions on Signal Processing. 61(2013)

[18] Zheng, J., and Zhou, X. "Three-Phase Composite Sphere Model for the Prediction of Chloride Diffusivity of Concrete." Materials in Civil Engineering 20(2008), 205-211.